Frontiers of Information Technology & Electronic Engineering
www.jzus.zju.edu.cn; engineering.cae.cn; www.springerlink.com
ISSN 2095-9184 (print); ISSN 2095-9230 (online)
E-mail: jzus@zju.edu.cn

Review:

Review of compact computational spectral information acquisition systems*

Hongya SONG[1], Wenyi ZHANG[1], Haifeng LI[1], Xu LIU[1,2,3], Xiang HAO[†‡1]

[1]*State Key Laboratory of Modern Optical Instrumentation, College of Optical Science and Engineering, Zhejiang University, Hangzhou 310027, China*

[2]*Ningbo Research Institute, Zhejiang University, Ningbo 315100, China*

[3]*Collaborative Innovation Center of Extreme Optics, Shanxi University, Taiyuan 030006, China*

[†]E-mail: haox@zju.edu.cn

Received May 27, 2019; Revision accepted Aug. 12, 2019; Crosschecked Mar. 24, 2020; Published online July 4, 2020

Abstract: With the development of computer science, more and more hardware implementations can be reproduced by software programming, bringing compact, cheap, and fast components to imaging instrumentation. In recent years, computational methods have been introduced into spectral detection, and computational spectrum acquisition implementations have emerged. This paper highlights the advantages of computational spectrum acquisition implementations by comparing them with traditional non-computational methods. Then, focusing on the compact feature, we review the most representative implementations, and finally make discussion and offer an outlook.

Key words: Spectral imaging; Computational imaging; Spectrometer
https://doi.org/10.1631/FITEE.1900266 **CLC number:** O433.1

1 Introduction

There has been a long history of spectral detection. The first spectral detection was made by Isaac Newton in 1665 (Newton, 1979), using triangular prism to divide sunlight into a rainbow-colored pattern. However, quantitative spectrum measurement was not possible until 1859 when the first practical spectrometer was developed by Kirchhoff and Bunsen (1861). In the 1960s, with the development of semiconductor and photoelectronic devices, the direct reading spectrometer was born, making it more convenient to store and process spectral data. Since the 1980s, with the arrival of two-dimensional (2D) charge coupled device (CCD) arrays, better optical design, improved electronics, and advanced manufacturing have all contributed to improving the performance by over an order of magnitude, bringing spectrum acquisition instrumentation into a prosperous era. Spectral imaging technology has been widely applied since that time (Hagen and Kudenov, 2013). However, conventional spectrometer and spectral imaging devices still suffer from many disadvantages, such as high cost, bulky volume, and heavy weight.

In recent years, with the development of computer science, more and more hardware implementations can be reproduced by software programming, bringing compact, cheap, and fast components to imaging instrumentation. As many computational methods have been introduced into spectral detection (Bangalore et al., 1996; Vigneau et al., 1997; Kurokawa et al., 2011; Rajwade et al., 2013), especially compressive sensing (Candès et al., 2006;

‡ Corresponding author

* Project supported by the National Key R&D Program of China (No. 2018YFA0701400), the Fundamental Research Funds for the Central Universities, China (No. 2019QNA5006), and the ZJU-Sunny Photonics Innovation Center, China (No. 2019-01)

ORCID: Hongya SONG, https://orcid.org/0000-0002-1995-4045; Xiang HAO, https://orcid.org/0000-0002-3931-6884

Donoho, 2006; Baraniuk, 2007; Candès and Wakin, 2008) and computational reconstruction algorithms, the original disadvantages are expected to be overcome. Moreover, a cheap, light, and small spectrum acquisition device can be widely applied, bringing down the threshold of spectrum detection to consumers. It has become possible to realize portable sensing systems even on smartphone platforms (Das et al., 2016).

Different kinds of computational spectral detection methods have been developed in recent years. In general, there are some sketchy principles for distinguishing whether a method is computational. First, computational spectral detection systems usually include spectral modulating or under sampling part for obtaining transformed spectral data. Second, complicated algorithms are adopted to extract spectral information from raw data. However, some non-computational implementations adopt more or less computational methods, such as de-noising algorithms, super-resolution methods, and/or data mapping. Before attempting the comparison of computational methods of spectral detection, it is necessary to make a clear definition of computational methods.

In this review, we are concerned with only those methods whose raw data can be understood by applying only a computational transform on it. Frankly speaking, the raw data acquired by system hardware looks nothing like the output data transformed by the software. This makes computation the kernel of the system, which distinguishes computational implementations from traditional spectral information acquisition systems. The schematic is shown in Fig. 1. Among the qualifying implementations, we further focus on those methods that have the potential to achieve compact-enclosure, light-weight, and ubiquitous spectrum detection.

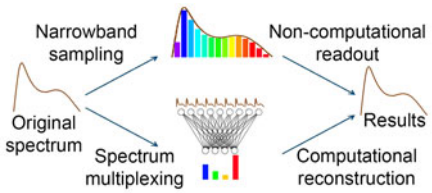

Fig. 1 Comparison of spectral detection using non-computational and computational methods

In this paper, we review many computational spectrometers and computational spectral imaging systems. Although traditional spectrometers and spectral imaging systems are rarely analyzed side by side because the physics behind them is different, in computational implementations, the principles are similar. Therefore, we treat both systems as computational spectral information acquisition systems.

2 Computational spectrometer

A spectrometer is the most typical instrument that detects the spectrum. It acquires one-dimensional (1D) spectral information. Based on the underlying operational principle, computational spectrometers can be classified as grating-based (Wolffenbuttel, 2004; Chaganti et al., 2006) and filter-based spectrometers.

2.1 Grating-based coded aperture spectrometer

As shown in Fig. 2, a traditional grating-based spectrometer consists of five parts, i.e., slit entrance, collimating optics, dispersive element (usually grating), focusing optics, and detector array (Wolffenbuttel, 2004). Based on the dispersive characteristic of the grating element, the hardware system samples a slit part of a test light source and forms a spanned spectrum distribution on a detector array plane. The spectrum shape is thus acquired by measuring the intensity distribution of dispersed light. However, there is a major trade-off in slit-based dispersion spectrometer design, i.e., spectral resolution versus light throughput. Increasing light throughput in a slit spectrometer while maintaining the spectral resolution requires a taller slit and detector, thus increasing the size and cost of the system (Cull et al., 2007). A design that maximizes spectrometer throughput without sacrificing spectral resolution is regarded as having a Jacquinot advantage (large area or throughput) (Jacquinot, 1960). Using coded aperture and computational methods, the trade-off can be broken.

In fact, the approach for realizing a coded aperture spectrometer has been carried out for a long time. In the early 1950s, Golay (1949, 1951) created the first coded aperture spectrometer, and Girard (1963) made some improvements. With the mathematical methods developed, Hadamard-transform (HT) spectrometers became the majority of coded aperture spectrometers (Decker, 1971; Hansen and Strong, 1972; Phillips and Briotta, 1974; Swift et al., 1976).

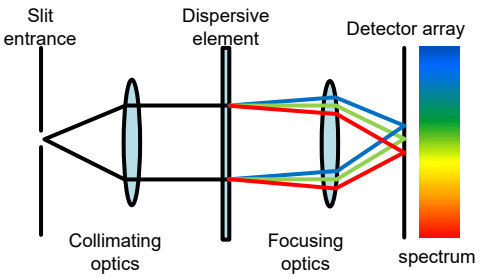

Fig. 2 Schematic of the traditional grating-based spectrometer

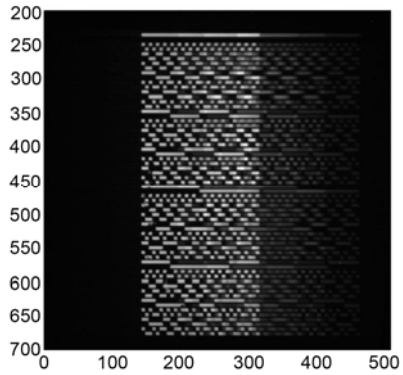

Fig. 3 Intensity image (distortion corrected) acquired by static MMS

Reprinted from Gehm et al. (2006), Copyright 2006, with permission from OSA

However, those HT spectrometers had only single-channel detectors or limited arrays of discrete detectors and a mask motion part. As a result, they are complicated and hard to miniaturize.

Gehm et al. (2006) presented a 2D coded aperture method that is optimized for the spectral characterization of diffuse sources, called a static multimodal and multiplex spectrometer (static MMS). Gehm et al. (2006) mathematically showed that 2D coding has to satisfy the orthogonality constraint. The design requirement can be met by basing the input aperture pattern on any family of orthogonal functions. Notably, the noise level intrinsically increases when the continuous mask codes (harmonic and Legendre basis) are applied as Parseval's relation does not hold. Therefore, the discrete codes are preferred. By replacing the slit with an orthogonal column code based on a row-doubled Hadamard matrix, the system simultaneously increased the light throughput and signal-to-noise ratio (SNR) without sacrificing spectral resolution. The distortion-corrected intensity image acquired through the coded aperture system is shown in Fig. 3. Compared with a slit spectrometer, the output increase of static MMS is about 10 times and the SNR increase is about 3.4 times.

Gehm et al. (2007) improved the static MMS by replacing the dispersive element with a hologram grating, and changed the detector array from a monochromatic CCD to a color one (Cull et al., 2007). The hologram grating was designed to have three different spectral bands, with the central wavelength corresponding to blue, green, and red lights. Unlike other designs of multiplexing spectrometers, the grating periods are set to disperse the spectral range of each band fully across the detector instead of separating spectral bands along the non-dispersing axis. Thus, the system was called a dispersion multiplexing spectrometer (DMS). These result in three spectral bands incident on the same detector pixels. Therefore, color CCD was selected to detect the spectrum. By separately reconstructing data from each color channel, the overlapped bands can be disambiguated. The data shifting induced by the spectral response difference between hologram grating and CCD Bayer filters was calibrated using a non-negative least-squares algorithm (Cull et al., 2007). The final detected spectrum was compared with that obtained by an Ocean Optics USB 2000 spectrometer (Fig. 4). Note that the peak locations can be resolved clearly. Right after DMS, Feller et al. (2007) (the same team as Gehm) attempted to change the coded aperture into a 37-ordered modified uniformly redundant array (MURA) and named the system "multi-order coded aperture" (MOCA). The spectrum detection result of a neon pen lamp was compared with that obtained by an Ocean Optics USB 2000 spectrometer (Fig. 5).

By applying multiplexing and computational reconstruction methods, the coded aperture spectrometer can measure an increased total spectral range with a small detector, which makes miniaturization easier. In fact, the DMS has a centimeter-sized shape (Fig. 6), which is comparable to the length of a key.

2.2 Filter-based computational spectrometer

The basic structure of a filter-based spectrometer is largely identical to that of a grating-based spectrometer, with a few minor differences. The hardware consists mainly of three parts, i.e., light collecting optics, filters, and detector(s). The light collecting part collects light rays from the test sample, making

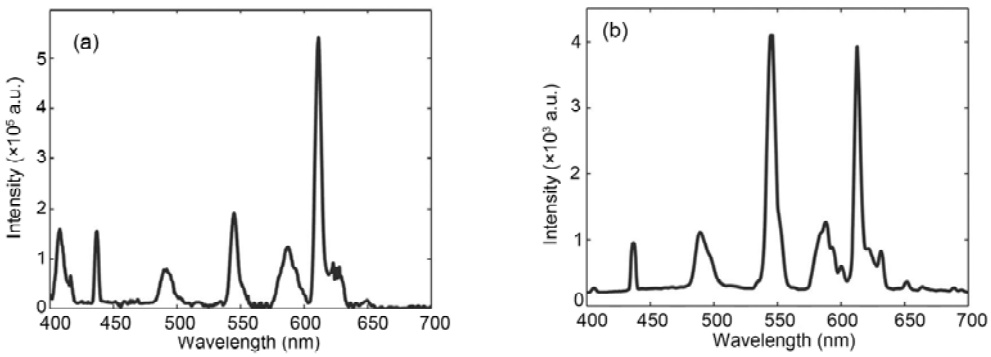

Fig. 4 Measurement result comparison between a dispersion multiplexing spectrometer (a) and a commercial spectrometer (b)
Reprinted from Cull et al. (2007), Copyright 2007, with permission from OSA

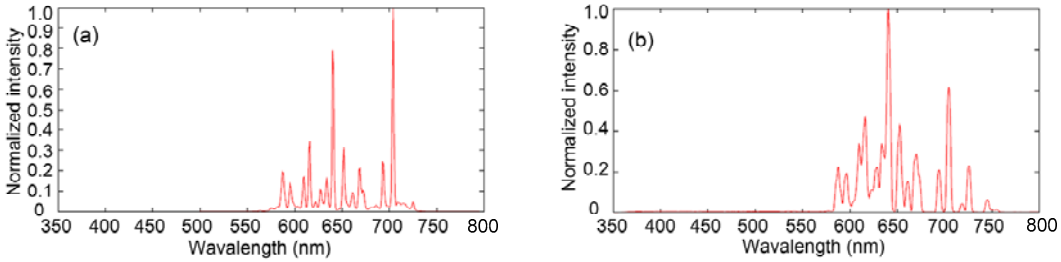

Fig. 5 Measurement results of a multi-order coded aperture (a) and a commercial spectrometer (b)
Reprinted from Feller et al. (2007), Copyright 2007, with permission from OSA

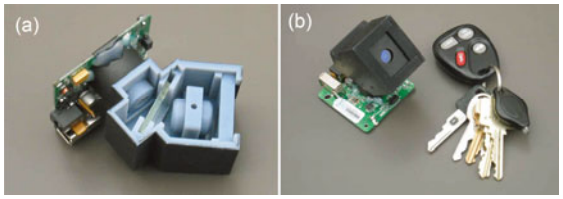

Fig. 6 Internal structure of the dispersion multiplexing spectrometer (DMS) (a) and DMS with keys to show the approximate size (b)
Reprinted from Cull et al. (2007), Copyright 2007, with permission from OSA

the optical parameters of incident light (such as incident angle, flux, and stray light level) more suitable for filtering and detection. When the light transmits through the filters, different wavelength components are separated sequentially or spatially. Finally, each component is measured by the detector or detector array, and thus the spectral information of the test sample is acquired by the system.

The most distinctive difference between computational and traditional spectrometers is the filter. Conventionally, bandpass filters are chosen to perform a wavelength decomposition task. To achieve higher spectral resolution, more filters with narrower passband are used. This strategy increases the volume and complexity of the whole system. Meanwhile, light throughput goes down when the spectral response curve gets narrow, resulting in a decreased SNR. In computational implementations, filters are broadband, which makes the raw data looks nothing like the original spectrum. However, by applying computational reconstruction algorithms, spectrum resolution can be resolved. Since broadband filters allow much more light to pass through, they allow the detection of the spectrum from a darker scene. Furthermore, according to the compressive sensing theory, it is possible to recover a sparse spectrum with a high probability using properly designed sensing filters, while the number of filters is much samller than that of the desired spectrum channels (recovering a higher-dimensional vector from a lower-dimensional vector), which is definitely a good approach for miniaturization. On the other hand, by applying a larger filter number, noise can be reduced using regularization algorithms (de-noising a lower-dimensional vector from a higher-dimensional vector),

which increases the SNR and makes the whole system more robust.

2.2.1 Low-cost thin-film spectrometer

Chang and Lee (2008) showed the achievability of a fine spectrometer on a chip based on a poor-performance and low-cost filter array. Fig. 7 shows the basic system model of the static filter array based spectrometer. An array of filters is directly placed on top of an array of photoelectric sensors such as CCD sensors. A filter may correspond to a CCD sensor or a group of CCD sensors. The outputs from the CCD sensors are then fed into a digital signal processor (Chang and Lee, 2008). Its hardware system structure is similar to that of a conventional filter-based spectrometer, and the only unique part is the spectral distribution curve of the filter array. As shown in Fig. 8, all filters are broadband and so-called low-cost filters. In the prototype system, the filter number is 40 and spectrum data is reconstructed by a non-negative constrained least-squares (NNLS) algorithm. Since Chang and Lee (2008) showed only the reconstruction results of a narrow-band Gaussian-shaped spectrum, we can conclude only that the prototype system can locate the center wavelength of a Gaussian-shaped spectrum at about 2 nm error level, while further quantitative evaluation cannot be carried out.

Chang et al. (2011b) improved their software implementation and made a sophisticated analysis of reconstruction accuracy. A Gaussian kernel template was adopted into the reconstruction approach for noise reduction, and the algorithm was improved into an l_1-norm minimization method. Comparisons were made among NNLS, the Tikhonov regularized non-negative least squares (TNNLS), and the l_1-norm algorithm in both simulation and real measurements. A broadband sample (tungsten halogen light filtered through colored plastic) was added into the measurement. In the same year, Chang et al. (2011a) increased the filter number to 119 and applied the system to accurate light emitting diode (LED) spectra measuring, achieving a mean absolute error of less than 1 nm for full width at half maximum (FWHM) and of less than 0.5 nm for center wavelength. The experiment presented the possibility of using a low-cost sensing system to match the performance of a laboratory quality optical spectrometer. However, it is noteworthy that the measurement accuracy level cannot represent the spectral resolution, since the system can handle only a single LED of a similar type. The measurement result depends highly on earlier stage training and selection of the Gaussian basis number, which limits application prospects.

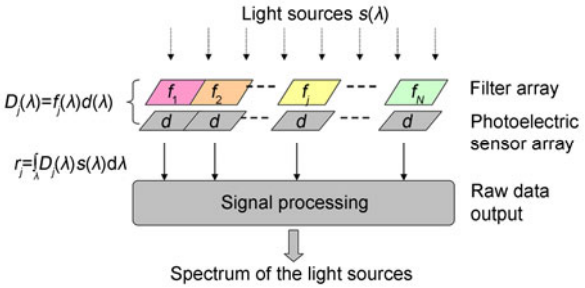

Fig. 7 Schematic of the filter array based spectrometer
Reprinted from Chang and Lee (2008), Copyright 2008, with permission from OSA

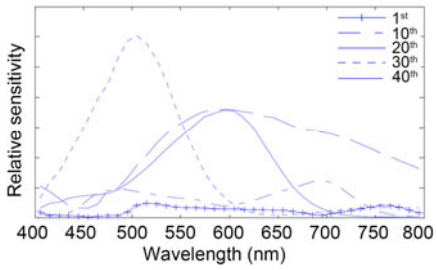

Fig. 8 Sensitivity responses of five spectral detectors among 40 low-cost filters
Reprinted from Chang and Lee (2008), Copyright 2008, with permission from OSA

Oliver et al. (2012) (the same team as Chang) exploited the sparse nature of a signal spectrum, showing that the resolution can be further improved beyond the limit set by the number of filters. Mirroring some of the works in compressive sensing (CS) (Candès et al., 2006; Donoho, 2006; Baraniuk, 2007; Candès and Wakin, 2008) with regard to the use of random matrices for signal acquisition and recovery, Oliver et al. (2013) redesigned the filters into a set of random transmittances. Using 40 filters, the reconstruction mean square error (MSE) was controlled at under −5 dB when the spectrum channel number N goes up to 405. Moreover, the resolution can be improved from 6.5 to 0.99 nm after filter redesign.

Notably, the resolution was derived from an MSE-based definition, which effectively represents the genie-aided MSE level of sparse signal reconstruction (Oliver et al., 2013). In other words, this

resolution result fits only specific spectrum measuring other than an arbitrary natural spectrum. However, the random thin-film filter (TF) design shows a 7-fold resolution improvement compared with low-cost TFs, and this is beneficial to spectrometer miniaturization.

Using a low-cost filter spectrometer structure and nanoimprint lithography technique, NanoLambda Inc. presented a miniaturized spectrometer product for skin tone measurement (Chang et al., 2014). The size of the main body part is only 7.5 mm×6.5 mm×5.7 mm. As shown in Fig. 9, the spectrometer is extremely small and could be held on a finger. Although the spectral reconstruction accuracy is not perfect, when applied to skin tone measurement, the color accuracy reaches an average Δxy of 0.0037 after *xyz* calibration, which is excellent for consumer use.

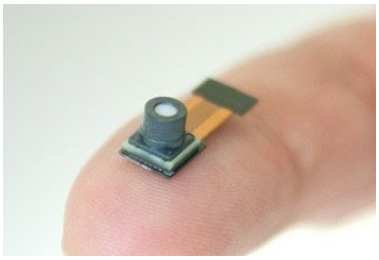

Fig. 9 Miniaturized spectrometer presented by NanoLambda Inc.

Reprinted from NanoLambda Inc. (https://nanolambda.myshopify.com), Copyright 2019, with permission from NanoLambda Inc.

2.2.2 Etalon-based spectrometer

In a broad sense, etalons have the spectrum filtering characteristic. Here, we treat the Fabry-Perrot etalon-based spectrometer as a kind of filter-based spectrometer. Since the etalon has a wavelength selectivity of multiple wavelengths, it can be categorized as a generalized broadband filter. A spectrometer which uses the broadband characteristic of etalons is a computational spectrometer. Traditionally, etalon-based spectrometers always contain a scanning mechanical part, which is a hindrance for miniaturization (Yetzbacher et al., 2014). Huang et al. (2017) presented a miniaturized method of etalon-array reconstructive spectrometry (EARS) by integrating etalons with different thicknesses in front of a CCD, realizing a compact hardware layout. The system structure is shown in Fig. 10.

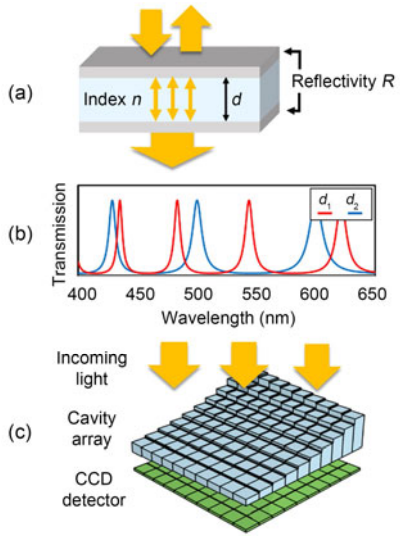

Fig. 10 System schematic of etalon-array reconstructive spectrometry: (a) an etalon consisting of two semi-reflecting surfaces with reflectivity *R* separated by an optically transparent medium of index *n* and thickness *d* (Light reflecting between the two surfaces interferes with itself, creating a characteristic transmission pattern); (b) two etalons of different thicknesses (d_1 and d_2) that will have uniquely encoded transmission patterns; (c) a CCD detector positioned under an etalon array with a unique thicknesses that will record the encoded light after it is transmitted through the etalons

Reprinted from Huang et al. (2017), Copyright 2017, with permission from Springer Nature, licensed under CC BY 4.0

In detail, the semi-reflecting surfaces are 30-nm silver films (reflection is about 0.7), and the optical spacing layer is a 700-nm SiO_2 layer under a 10×10 PMMA step-structure with a thicknesses of 0.8–2.8 μm, for a total cavity thickness variation of 1.5–3.5 μm in 100 steps (Huang et al., 2017). The cavity array was placed above the CCD sensor. The achievable resolution is determined by the thickness range and finesse of the etalons. The EARS system reaches a sampling period of 4 nm, and equivalently offers a spectral resolution of 8 nm under the Nyquist sampling principle. However, if the signal is known to be sparse on a particular basis, by adopting the nature of compressive sensing, the resolution could exceed the resolution limit. For example, if the signal is known to be a laser source, the wavelength center positional accuracy is as high as 0.12 nm.

The cavity array makes the EARS system a step further on the road to miniaturization. As presented in Fig. 11, the size of the cavity array is 5 mm×5 mm, smaller than a dime. However, the experimental setup

is still large-sized for better light control and better measurement performance (Huang et al., 2017). By applying a complementary metal oxide semiconductor (CMOS) compatible fabrication process of Fabry-Perot resonators, a single-chip optical spectrometer can be realized (Correia et al., 2000).

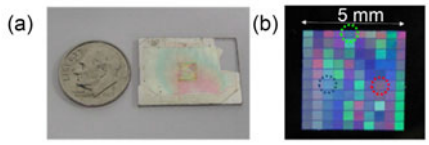

Fig. 11 Photograph of the cavity array in an etalon-array reconstructive spectrometry: (a) a photo of the fabricated 10×10 etalon array next to a dime for scale; (b) a color photograph of the etalon array back-illuminated by room fluorescent lighting, showing cavity-dependent color transmission

Reprinted from Huang et al. (2017), Copyright 2017, with permission from Springer Nature, licensed under CC BY 4.0

2.2.3 New material filter spectrometer

The development of material science and nano-manufacturing technology brings more degrees of freedom for physical variable manipulation, and spectral modulation achieves many new approaches. New material-based methods overcome some of the limitations brought by traditional manufacturing, broadening the boundary of spectral detection. Here, we briefly introduce several representative new material based filter spectrometer implementations.

1. Quantum dot spectrometer

Bao and Bawendi (2015) presented a broadband quantum dot filter based spectrometer. By replacing interferometric optics with a 2D absorptive filter array composed of 195 colloidal quantum dots (CQDs), the miniaturized spectrometer reaches a spectral resolution of 1 nm with a measurement range of 300 nm. Owing to the similar basic structure, the quantum dot spectrometer shares all advantages with the broadband filter spectrometer. The spectrum channel number and spectral range can be increased simultaneously by increasing the number of different CQDs used in the filter array without sacrificing the total photon efficiency. Furthermore, due to the spectral isotropy property of the quantum dot material, a quantum dot spectrometer can analyze the light from a source with a wide angular distribution while maintaining the spectral resolution, which is a challenge for a traditional filter based spectrometer due to a high angle sensitivity of optical filters.

The spectrum reconstruction measurement results are shown in Fig. 12. The quantum dot spectrometer can reproduce all the major features of the spectra. The quantum dot spectrometer works on the basis of light absorption characteristics, which is the most reliable property of CQDs. This not only makes it more environment-friendly, but also increases the stability, which is very critical for a commercial spectrometer.

CQD filter arrays are fabricated by tightly printing small drops of CQD/PVB solutions close together onto a glass cover slip with an automatic pipette. Fig. 13 shows the CQD filter array. Each dot is a CQD filter made of one type of CQD material embedded in a polyvinyl butyral thin film. The size of each filter is about 0.5 mm across. As shown in Fig. 14, a quantum dot micro-spectrometer in the form of a digital camera with electronics and circuits has a size comparable to that of a US quarter.

2. Plasmonic metasurface spectrometer

Metasurfaces has been a hot spot research topic recently, and metasurface-based spectrometry has been developed. Most developments use metasurfaces as dispersive elements to split different wavelength components (Li et al., 2015; Shaltout et al., 2015; Faraji-Dana et al., 2018). Craig et al. (2018) developed a plasmonic metasurface based spectrometer, using an array of plasmonic metasurfaces (Fig. 15) that act as broadband filters for spectrum modulation. The light emitted from the test sample transmits through the filter array plate, and the intensity behind each antenna is measured. Using a recursive least-squares (RLS) algorithm (Hayes, 1996), the spectrum of the test sample is finally determined.

Each metasurface filter consists of a square array of gold blocks on a double-sided polished undoped silicon (Si) substrate. Thinking about the gold blocks as resonant antennas (Crozier et al., 2003; Adato et al., 2009; Kats et al., 2013), one would expect a dip in transmission under a certain wavelength, while the resonant wavelength is proportional to the antenna length. By varying the period of antennas in each filter unit cell, a metasurface filter array with different spectral transmittances can be manufactured. Fig. 16 shows the transmission spectra of all 116 filters. It can be seen that those filters are all broadband filters.

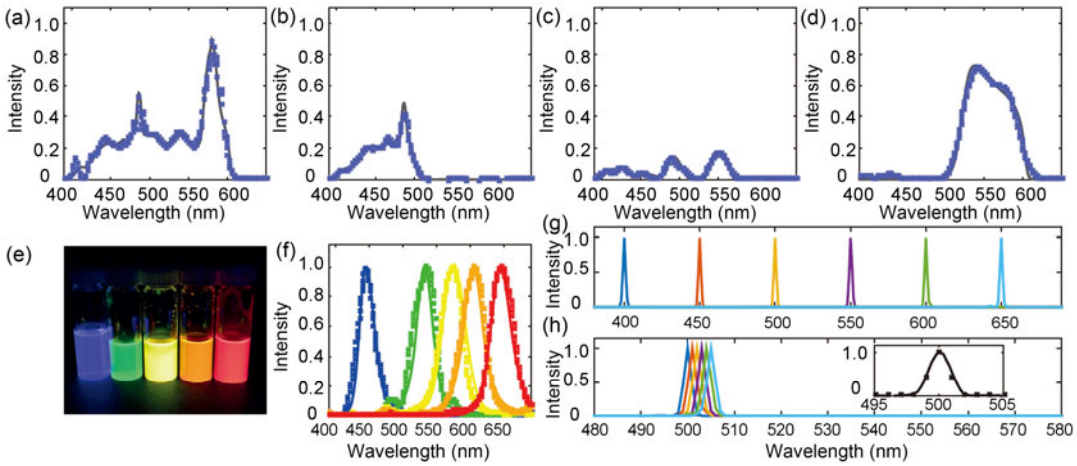

Fig. 12 Quantum dot spectrometer measurements: (a–d) quantum dot spectrometer measurements of broadband spectra (crosses) and reference spectra (solid lines) using a commercial spectrometer; (e) fluorescent emission of five CQD samples under ultraviolet excitation; (f) measurements (markers) using the quantum dot spectrometer of the emission spectra of the five CQD samples shown in (e), and reference spectra (solid lines) using a spectrofluorometer; (g, h) measurements of monochromatic light spectra

The peak positions of the six monochromatic lights in (g) are 400, 450, 500, 550, 600, and 650 nm. The peak positions of the six monochromatic lights in (h) are 500, 501, 502, 503, 504, and 505 nm. The inset of (h) compares the measured spectrum of the 500 nm monochromatic light with crosses and the reference spectrum with solid line. Reprinted from Bao and Bawendi (2015), Copyright 2015, with permission from Springer Nature

Fig. 13 Colloidal quantum dot (CQD) materials in the form of filters

Each dot is a CQD filter made of one type of CQD material embedded in a polyvinyl butyral thin film. Reprinted from Bao and Bawendi (2015), Copyright 2015, with permission from Springer Nature

Fig. 14 A quantum dot micro-spectrometer in the form of a digital camera with electronics and circuits

Reprinted from Bao and Bawendi (2015), Copyright 2015, with permission from Springer Nature

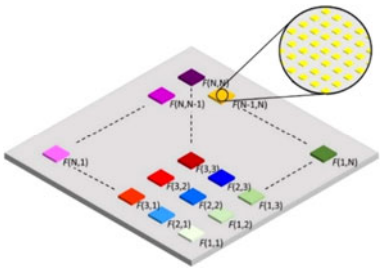

Fig. 15 Schematic of the filter array in a plasmonic metasurface spectrometer

Reprinted from Craig et al. (2018), Copyright 2018, with permission from OSA

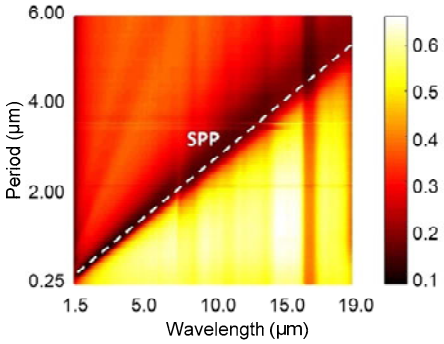

Fig. 16 Measured transmission spectra for all 116 filters in a plasmonic metasurface spectrometer

Reprinted from Craig et al. (2018), Copyright 2018, with permission from OSA

The reconstruction results are shown in Fig. 17. The plasmonic metasurface spectrometer offers a broad spectral detection range over the short- to long-wave infrared (1.5–19 μm), which is far beyond that of miniaturized spectrometers. However, the intensity is detected by a Fourier-transform infrared (FTIR) spectrometer because of the difficulty of manufacturing a miniaturized and broadband infrared detector array, making the plasmonic metasurface spectrometer only a proof-of-concept system. The future integration of the filter array with such a detector array could form the basis for light-weight, portable, and inexpensive infrared spectrometers (Craig et al., 2018).

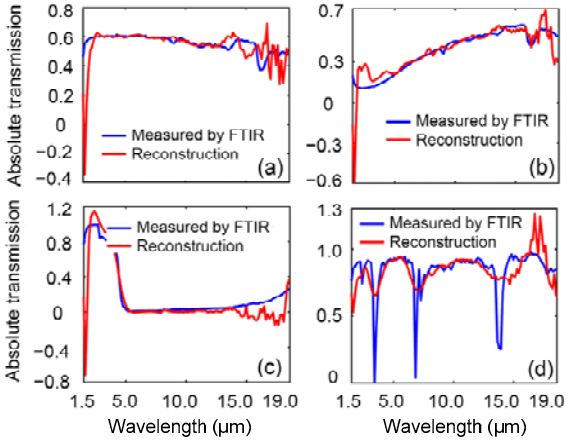

Fig. 17 Reconstruction results of a plasmonic metasurface spectrometer generated by passing light from the globar through double-sided polished undoped silicon (Si) (a), single-sided polished doped Si (b), glass (c), and polyethylene (d)

Reprinted from Craig et al. (2018), Copyright 2018, with permission from OSA

3. Photonic crystal slab spectrometer

Photonic crystal (PC) material is a hotspot in the research field. PC has been applied into spectrum detection during past decades (Wolffenbuttel, 2004; Momeni et al., 2009; Pervez et al., 2010; Redding et al., 2013; Kita et al., 2018). However, most of these implementations are waveguide coupled, which limits the detection flexibility (due to the strict angular coupling restriction). Wang Z et al. (2019) presented a free-space coupled on-chip spectrometer based on photonic crystal slabs. They claimed this to be completely CMOS compatible and mass producible at low cost.

Briefly, the working principle of a PC slab spectrometer is that simple PC slabs play the role of an optical resonator which modulates the spectrum, and that the CMOS detector measures the intensity. By fabricating a PC slab array with different periodicities, lattice constants, and hole sizes on top of a CMOS imaging sensor, a PC slab spectrometer can be made. However, unlike microcavities, PC slabs create a transmission spectrum with rich spectral features because of the multiple resonance effects. The detected spectrum has to be reconstructed by computational algorithms. Wang Z et al. (2019) adopted a regularized linear regression algorithm for spectrum reconstruction. The system structure is shown in Fig. 18, while the reconstruction results are shown in Fig. 19.

In Fig. 18, the PC slab spectrometer is extremely small. Each of the spectrometer is around 200 μm on a side. Wang Z et al. (2019) demonstrated the potential of PC slab spectrometers for single-shot hyperspectral

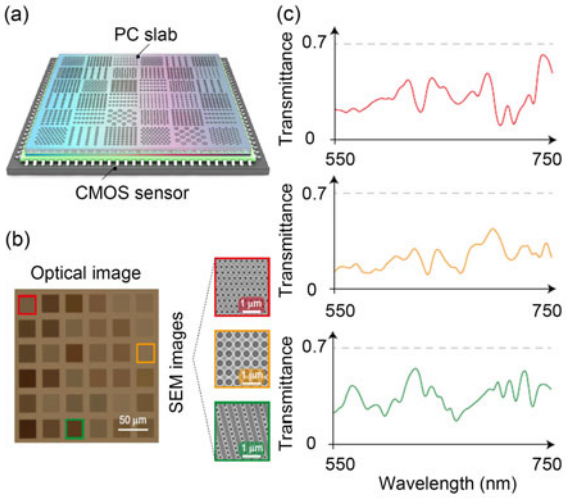

Fig. 18 Micro-spectrometer based on photonic crystal (PC) slabs: (a) schematic of the spectrometer, which consists of an array of PC slabs with different parameters; (b) optical image of the fabricated 6×6 PC structures; (c) measured transmission spectra $T(\lambda)$ of the three structures in (b)

In (a), these slabs are integrated on top of a CMOS sensor array. In (b), three scanning electron microscopy (SEM) images of selected PC slab structures marked by red, orange, and green frames are shown on the side. In (c), for each PC slab, the corresponding $T(\lambda)$ is characterized using a monochromator. References to color refer to the online version of this figure. Reprinted from Wang Z et al. (2019), Copyright 2019, with permission from Springer Nature, licensed under CC BY 4.0

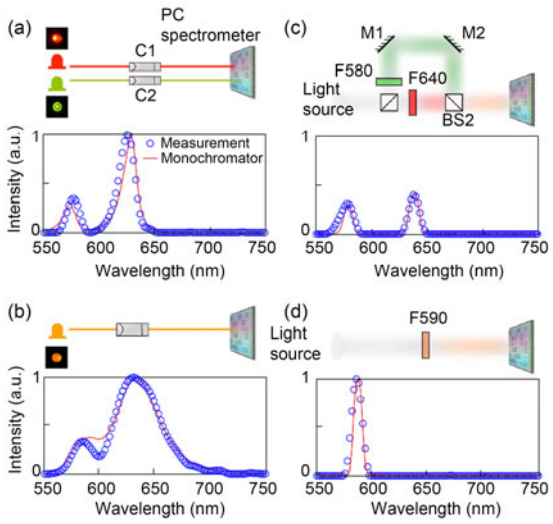

Fig. 19 Recovery of broadband spectra: (a) measurement of the emission spectrum of a combination of two LEDs (green and red); (b) measurement of the emission spectrum of a multimode LED (orange/red); (c) measurement of a white light beam passing through two filters; (d) measurement of a white light beam passing through a single bandpass filter

The appearance color of the filtered light in (d) is the same as that of the recombined light in (c). For all four cases, the measurement results using the PC spectrometer (circled lines) match well the reference spectra obtained by a commercial monochromator (red solid line). M: mirror; F: filter; BS: beam splitter. References to color refer to the online version of this figure. Reprinted from Wang Z et al. (2019), Copyright 2019, with permission from Springer Nature, licensed under CC BY 4.0

hyperspectral imaging by fabricating 10×10 identical spectrometers on a silicon-on-sapphire substrate.

PC slabs can be fabricated via single exposure photolithography and require only standard CMOS materials. As the spectral response functions are entirely extrinsic and are enabled by structures instead of material properties, the concept can be applied to any wavelength range by scaling the dimension of the PC, giving this implementation an important potential for the miniaturized spectrometer.

3 Computational spectral imaging

Compared with spectrometers, spectral imaging acquires a 3D data cube that involves spatial (x, y) and spectral (λ) information. A spatial resolution makes spectral data more intuitive. Therefore, one can conveniently acquire the spatial distribution of spectral information. Spatial distribution information may be more important than a high spectral resolution in certain applications, such as geological survey and crop disease assessment. However, the acquisition of 3D information is a complicated task, because spatial and spectral data is usually acquired through different methods, and the simultaneous acquisition for spatial and spectral data increases system complexity. Traditional spectral imaging methods multiplex spatial and spectral dimension by adopting either time division or space division, which brings trade-offs between spectral and spatial resolutions (or frame rate).

To address the above problems, computational methods can be applied. With the development of compressive sensing theory, the acquired data can be highly compressed. Here, we categorize computational spectral imaging methods into two parts, i.e., computation (or specifically, compression) in the spectral (λ) dimension and computation in the spatial (x, y) dimension. In this section, we focus on those implementations that adopt computational methods to realize a miniaturized and ubiquitous spectral imaging system.

3.1 Computation in spectral (λ) dimension

The most straightforward way to transform spectrometry into a spectral imaging device is to directly use a spectrometer to acquire the spectrum of each pixel and then combine the data into a spectral image. By applying computational methods, spatial or temporal work on spectrum detection can be compressed, and the spatial resolution or frame rate will be improved dramatically. In fact, any imaging methods using spectrometers in Section 2 can be regarded as computational spectral imaging that carries out computation in the spectral dimension. However, computational spectrometers are usually invented afresh, and there are few attempts for spectral imaging. The only exception mentioned in Section 2 is the PC slab spectrometer, realizing a spatial resolution of 10×10 pixels, which is not comparable to those of traditional imaging spectrometers. Moreover, a spatial scanning imaging system usually contains moving parts like galvanometers, which are fragile.

Among implementations without moving parts, the snapshot hyperspectral imaging Fourier transform

(SHIFT) spectrometer (Kudenov and Dereniak, 2012) may be considered a computational method, as the reconstruction process is necessary for spectrum detection. However, the spectral information is not compressed, because the reconstruction is carried out by the Fourier transform.

1. Computed tomography imaging spectrometry

A typical computational approach is the computed tomography imaging spectrometry (CTIS). This concept was independently invented by Okamoto and Yamaguchi (1991) and Bulygin and Vishnyakov (1992). After years of development, the first high-resolution CTIS was developed by Ford et al. (2001). Using a 2048×2048 CCD camera, the spatial resolution reached 203×203 pixels and the spectral channel number was 55. In CTIS systems (Fig. 20), the mixing of spatial and spectral data varies at different positions on the detector by adopting a 2D dispersion element. The aliasing compresses the spectral and spatial data into a single shot, and the spectral image can be reconstructed by tomographic algorithms. In this way, the system layout becomes more compact.

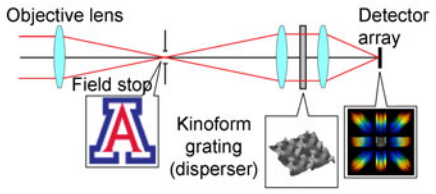

Fig. 20 System layout of a computed tomography imaging spectrometer

Reprinted from Hagen and Kudenov (2013), Copyright 2013, with permission from SPIE, licensed under CC BY 3.0

However, non-coded aliasing, calibration difficulty, and measurement artifacts result in a relatively poor spectral performance, and the difficulty in manufacturing the kinoform disperser hinders the CTIS system from wide use (Hagen and Kudenov, 2013).

2. HyperCam

Goel et al. (2015) designed a product named "HyperCam" for ubiquitous spectral imaging. It has a simple system structure, i.e., a 17-LED light source, a driver board, and a CMOS camera (Photo of the system is available from Goel et al. (2015)). Each part is of low cost and is designed for consumer use. The frame rate goes from 9 to 150 frames/s depending on the number of channels used, and the spatial resolution is 1280×1024.

The narrowband LEDs were empirically selected to cover the camera sensitivity range. The spectral power distribution curves of LEDs are available from Goel et al. (2015). These spectral curves can be regarded as poor conditions in traditional spectral detection, and thus the spectral resolution is not expected to be high. Instead of pursuing spectral reconstruction accuracy, Goel et al. (2015) optimized the system in an application-oriented way. Much software computational work has been done for two different applications, i.e., user-specific feature acquisition in a multi-user interaction system and food monitoring.

In the first application, the multi-channel image was acquired and then computed to form an immersed image that emphasizes the hand feature. Through the evaluation, we can see that this approach is successful at reliable distinguishment between five users at a time, which is suitable for most multi-touch surface systems. The second application is more familiar and the system correctly predicted relative ripeness at an accuracy of 94% (while the accuracy is only 62% using the RGB images) (Goel et al., 2015).

The design of HyperCam shows the possibility of ubiquitous spectral imaging. Although the spectral performance of such devices is not promising, we believe that with the development of hardware design and machine learning algorithms, low-cost spectral imaging devices may be widely used in specific recognition applications.

3.2 Computation in spatial (x, y) dimension

Following the appearance of the single pixel imaging concept (Takhar et al., 2006; Duarte et al., 2008) derived from compressive sensing (Candès et al., 2006; Donoho, 2006; Baraniuk, 2007; Candès and Wakin, 2008), a new imaging scheme has been developed to acquire an image with compressed sampling. Using a spatial light modulator (SLM) to generate changeable spatial coding, the image can be reconstructed from a single pixel detector by adopting an l_1-norm minimization algorithm. Moreover, the acquired data can be extremely compressed if the scene is somehow "sparse," and this is beneficial to spectral imaging. Using a spectrometer as a single pixel detector, a spectral image can be acquired under this structure. Attempts have been made during the

last decade (Sun and Kelly, 2009; Soldevila et al., 2013; Kuiteing et al., 2014).

The earliest and most representative implementation is the coded aperture snapshot spectral imager (CASSI) system. Unlike single pixel imaging, the CASSI system develops a different structure and makes better use of compressive sensing for spectral imaging. The concept of CASSI was derived from the coded-aperture spectrometer (Gehm et al., 2007; Willett et al., 2007; Wagadarikar et al., 2008). As introduced in Section 2.1, a static MMS allows de-multiplexing during reconstruction processing without sacrificing the spectral resolution by taking a column orthogonal matrix as a coded mask. Adopting compressive sensing theory, the coded mask is changed into a random binary matrix, and the reconstruction algorithm becomes more complicated. As shown in Fig. 21, the major components of the CASSI system are similar to those of the static MMS. A coded aperture mask modulates a data cube into a randomly hollowed shape in the spatial dimension, and a dispersive element shifts the cube across the wavelength dimension. The 2D detector array measures the intensity image, which is formed by projecting the shifted data cube along the wavelength dimension. If this code satisfies the requirements of compressive sensing, then the object data cube can be sufficiently estimated using compressive sensing reconstruction algorithms (Gehm et al., 2007). With proper hardware design, the whole system can be made compact, and the acquired data is highly compressed due to the use of the compressive sensing method. Furthermore, this snapshot imaging system can realize a capture ability of the video frame rate with a resolution at the same order as the detector. Wagadarikar et al. (2009) showed that CASSI can capture 248×248×33 data cubes at 30 frames/s.

A number of improved CASSI systems emerged after the presentation of the prototype, such as dual-camera design for improving resolution and reducing reconstruction complexity (Wang LZ et al., 2015, 2017), colored coded aperture design for improving spectral compression efficiency (Arguello and Arce, 2014; Rueda et al., 2015; Hinojosa et al., 2016; Diaz et al., 2018), code aperture pattern optimization for increasing spatial resolution and reconstruction speed (Arguello and Arce, 2011), reconstruction algorithm improvement for specific scene applications

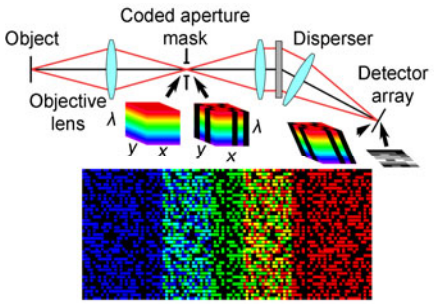

Fig. 21 Schematic of the coded aperture snapshot spectral imager (CASSI) system

Top: system layout for a CASSI, showing only the single-disperser configuration. Bottom: pattern on the detector array due to imaging a coded aperture mask through a disperser for an object that emits only three wavelengths (the wavelengths used in the example image here are the shortest, middle, and longest wavelengths detected by the system). Reprinted from Hagen and Kudenov (2013), Copyright 2013, with permission from SPIE, licensed under CC BY 3.0

(Arguello et al., 2013; Rajwade et al., 2013; Galvis et al., 2017), and hardware extension for multidimensional imaging (Gao and Wang, 2016; Ren et al., 2018). CASSI and the underlying mathematical methods have developed a lot during the past decade, and we expect this method to be a potential approach for ubiquitous spectral imaging.

4 Conclusions

Spectral information acquisition technology has developed rapidly over past decades. Thanks to the application of new materials and computational algorithms, many new implementations have emerged, showing us new possibilities in spectrometers and spectral imaging. Compared with traditional devices, most of computational spectroscopy devices may still work at low accuracy. However, from the view of ubiquitous applications, such as smartphone-based detection or spectrum-based recognition, this defect becomes less critical. Instead, these methods are highlighted by their low cost, light weight, and compact enclosures. These advantages are always more attractive than pursuing a perfect performance in such applications. Efforts have been made in recent years for consumer used spectral detection. We believe that the co-design of hardware and the computational algorithm will lead to the wide use of spectral

information, and that with the developments of the Internet of Things (IoT) and artificial intelligence (AI), ubiquitous spectrometers and spectral imaging will bring benefit to humankind.

Contributors

Haifeng LI and Xu LIU guided the investigation. Hongya SONG, Wenyi ZHANG, and Xiang HAO investigated the main information. Hongya SONG summarized the information and drafted the manuscript. Wenyi ZHANG and Xiang HAO helped organize the manuscript. Hongya SONG and Xiang HAO revised and finalized the paper.

Compliance with ethics guidelines

Hongya SONG, Wenyi ZHANG, Hai-feng LI, Xu LIU, and Xiang HAO declare that they have no conflict of interest.

References

Adato R, Yanik AA, Amsden JJ, et al., 2009. Ultra-sensitive vibrational spectroscopy of protein monolayers with plasmonic nanoantenna arrays. *PNAS*, 106(46):19227-19232. https://doi.org/10.1073/pnas.0907459106

Arguello H, Arce GR, 2011. Code aperture optimization for spectrally agile compressive imaging. *J Opt Soc Am A*, 28(11):2400-2413. https://doi.org/10.1364/josaa.28.002400

Arguello H, Arce GR, 2014. Colored coded aperture design by concentration of measure in compressive spectral imaging. *IEEE Trans Image Process*, 23(4):1896-1908. https://doi.org/10.1109/tip.2014.2310125

Arguello H, Correa CV, Arce GR, 2013. Fast lapped block reconstructions in compressive spectral imaging. *Appl Opt*, 52(10):D32-D45. https://doi.org/10.1364/ao.52.000d32

Bangalore AS, Shaffer RE, Small GW, et al., 1996. Genetic algorithm-based method for selecting wavelengths and model size for use with partial least-squares regression: application to near-infrared spectroscopy. *Anal Chem*, 68(23):4200-4212. https://doi.org/10.1021/ac9607121

Bao J, Bawendi MG, 2015. A colloidal quantum dot spectrometer. *Nature*, 523(7558):67-70. https://doi.org/10.1038/nature14576

Baraniuk RG, 2007. Compressive sensing. *IEEE Signal Process Mag*, 24(4):118-121. https://doi.org/10.1109/msp.2007.4286571

Bulygin TV, Vishnyakov GN, 1992. Spectrotomography: a new method of obtaining spectrograms of two-dimensional objects. Analytical Methods for Optical Tomography, p.315-323. https://doi.org/10.1117/12.131904

Candès EJ, Wakin MB, 2008. An introduction to compressive sampling. *IEEE Signal Process Mag*, 25(2):21-30. https://doi.org/10.1109/msp.2007.914731

Candès EJ, Romberg J, Tao T, 2006. Robust uncertainty principles: exact signal reconstruction from highly incomplete frequency information. *IEEE Trans Inform Theory*, 52(2):489-509. https://doi.org/10.1109/tit.2005.862083

Chaganti K, Salakhutdinov I, Avrutsky I, et al., 2006. A simple miniature optical spectrometer with a planar waveguide grating coupler in combination with a plano-convex lens. *Opt Expr*, 14(9):4064-4072. https://doi.org/10.1364/oe.14.004064

Chang CC, Lee HN, 2008. On the estimation of target spectrum for filter-array based spectrometers. *Opt Expr*, 16(2):1056-1061. https://doi.org/10.1364/oe.16.001056

Chang CC, Chen CC, Kurokawa U, et al., 2011a. Accurate sensing of LED spectra via low-cost spectrum sensors. *IEEE Sens J*, 11(11):2869-2877. https://doi.org/10.1109/jsen.2011.2147302

Chang CC, Lin NT, Kurokawa U, et al., 2011b. Spectrum reconstruction for filter-array spectrum sensor from sparse template selection. *Opt Eng*, 50(11):114402. https://doi.org/10.1117/1.3645086

Chang CC, Chuang YC, Wu CT, et al., 2014. A low-cost mobile device for skin tone measurement using filter array spectrum sensor. Sensors, p.499-502. https://doi.org/10.1109/ICSENS.2014.6985044

Correia J, de Graaf G, Kong SH, et al., 2000. Single-chip CMOS optical microspectrometer. *Sens Actuat A Phys*, 82(1-3):191-197. https://doi.org/10.1016/s0924-4247(99)00369-6

Craig B, Shrestha VR, Meng JJ, et al., 2018. Experimental demonstration of infrared spectral reconstruction using plasmonic metasurfaces. *Opt Lett*, 43(18):4481-4484. https://doi.org/10.1364/ol.43.004481

Crozier KB, Sundaramurthy A, Kino GS, et al., 2003. Optical antennas: resonators for local field enhancement. *J Appl Phys*, 94(7):4632-4642. https://doi.org/10.1063/1.1602956

Cull EC, Gehm ME, Brady DJ, et al., 2007. Dispersion multiplexing with broadband filtering for miniature spectrometers. *Appl Opt*, 46(3):365-374. https://doi.org/10.1364/ao.46.000365

Das AJ, Wahi A, Kothari I, et al., 2016. Ultra-portable, wireless smartphone spectrometer for rapid, non-destructive testing of fruit ripeness. *Sci Rep*, 6:32504. https://doi.org/10.1038/srep32504

Decker JA, 1971. Experimental realization of the multiplex advantage with a Hadamard-transform spectrometer. *Appl Opt*, 10(3):510-514. https://doi.org/10.1364/AO.10.000510

Diaz N, Rueda H, Arguello H, 2018. Adaptive filter design via a gradient thresholding algorithm for compressive spectral imaging. *Appl Opt*, 57(17):4890-4900. https://doi.org/10.1364/AO.57.004890

Donoho DL, 2006. Compressed sensing. *IEEE Trans Inform Theory*, 52(4):1289-1306. https://doi.org/10.1109/tit.2006.871582

Duarte MF, Davenport MA, Takhar D, et al., 2008. Single-pixel imaging via compressive sampling. *IEEE Signal Process Mag*, 25(2):83-91.

https://doi.org/10.1109/msp.2007.914730

Faraji-Dana M, Arbabi E, Arbabi A, et al., 2018. Compact folded metasurface spectrometer. *Nat Commun*, 9(1): 4196. https://doi.org/10.1038/s41467-018-06495-5

Feller SD, Chen H, Brady DJ, et al., 2007. Multiple order coded aperture spectrometer. *Opt Expr*, 15(9):5625-5630. https://doi.org/10.1364/OE.15.005625

Ford BK, Descour MR, Lynch RM, 2001. Large-image-format computed tomography imaging spectrometer for fluorescence microscopy. *Opt Expr*, 9(9):444-453. https://doi.org/10.1364/oe.9.000444

Galvis L, Lau D, Ma X, et al., 2017. Coded aperture design in compressive spectral imaging based on side information. *Appl Opt*, 56(22):6332-6340. https://doi.org/10.1364/ao.56.006332

Gao L, Wang LV, 2016. A review of snapshot multidimensional optical imaging: measuring photon tags in parallel. *Phys Rep*, 616:1-37. https://doi.org/10.1016/j.physrep.2015.12.004

Gehm ME, McCain ST, Pitsianis NP, et al., 2006. Static two-dimensional aperture coding for multimodal, multiplex spectroscopy. *Appl Opt*, 45(13):2965-2974. https://doi.org/10.1364/ao.45.002965

Gehm ME, John R, Brady DJ, et al., 2007. Single-shot compressive spectral imaging with a dual-disperser architecture. *Opt Expr*, 15(21):14013-14027. https://doi.org/10.1364/oe.15.014013

Girard A, 1963. Spectromètre à grilles. *Appl Opt*, 2(1):79-87 (in French). https://doi.org/10.1364/ao.2.000079

Goel M, Whitmire E, Mariakakis A, et al., 2015. HyperCam: hyperspectral imaging for ubiquitous computing applications. Proc ACM Int Joint Conf on Pervasive and Ubiquitous Computing, p.145-156. https://doi.org/10.1145/2750858.2804282

Golay MJE, 1949. Multi-slit spectrometry. *J Opt Soc Am*, 39(6):437-444. https://doi.org/10.1364/josa.39.000437

Golay MJE, 1951. Static multislit spectrometry and its application to the panoramic display of infrared spectra. *J Opt Soc Am*, 41(7):468-472. https://doi.org/10.1364/josa.41.000468

Hagen NA, Kudenov MW, 2013. Review of snapshot spectral imaging technologies. *Opt Eng*, 52(9):090901. https://doi.org/10.1117/1.oe.52.9.090901

Hansen P, Strong J, 1972. High resolution Hadamard transform spectrometer. *Appl Opt*, 11(3):502-506. https://doi.org/10.1364/AO.11.000502

Hayes MH, 1996. Statistical Digital Signal Processing and Modeling. John Wiley & Sons, New York, USA.

Hinojosa CA, Correa CV, Arguello H, et al., 2016. Compressive spectral imaging using multiple snapshot colored-mosaic detector measurements. Computational Imaging, Article 987004. https://doi.org/10.1117/12.2224369

Huang E, Ma Q, Liu ZW, 2017. Etalon array reconstructive spectrometry. *Sci Rep*, 7:40693. https://doi.org/10.1038/srep40693

Jacquinot P, 1960. New developments in interference spectroscopy. *Rep Prog Phys*, 23(1):267-312. https://doi.org/10.1088/0034-4885/23/1/305

Kats MA, Blanchard R, Genevet P, et al., 2013. Thermal tuning of mid-infrared plasmonic antenna arrays using a phase change material. *Opt Lett*, 38(3):368-370. https://doi.org/10.1364/ol.38.000368

Kirchhoff GR, Bunsen RW, 1861. Chemische analyse durch spectralbeobachtungen. *Ann Phys Chem*, 189:3370381 (in German). https://doi.org/10.1002/andp.18611890702

Kita DM, Miranda B, Favela D, et al., 2018. High-performance and scalable on-chip digital Fourier transform spectroscopy. *Nat Commun*, 9(1):4405. https://doi.org/10.1038/s41467-018-06773-2

Kudenov MW, Dereniak EL, 2012. Compact real-time birefringent imaging spectrometer. *Opt Expr*, 20(16):17973-17986. https://doi.org/10.1364/oe.20.017973

Kuiteing SK, Coluccia G, Barducci A, et al., 2014. Compressive hyperspectral imaging using progressive total variation. IEEE Int Conf on Acoustics, Speech and Signal Processing, p.7794-7798. https://doi.org/10.1109/ICASSP.2014.6855117

Kurokawa U, Choi BI, Chang CC, 2011. Filter-based miniature spectrometers: spectrum reconstruction using adaptive regularization. *IEEE Sens J*, 11(7):1556-1563. https://doi.org/10.1109/jsen.2010.2103054

Li ZY, Palacios E, Butun S, et al., 2015. Visible-frequency metasurfaces for broadband anomalous reflection and high-efficiency spectrum splitting. *Nano Lett*, 15(3): 1615-1621. https://doi.org/10.1021/nl5041572

Momeni B, Hosseini ES, Askari M, et al., 2009. Integrated photonic crystal spectrometers for sensing applications. *Opt Commun*, 282(15):3168-3171. https://doi.org/10.1016/j.optcom.2009.04.052

Newton I, 1979. Opticks (2nd Ed.). Dover Publications Inc., New York, USA.

Okamoto T, Yamaguchi I, 1991. Simultaneous acquisition of spectral image information. *Opt Lett*, 16(16):1277-1279. https://doi.org/10.1364/ol.16.001277

Oliver J, Lee W, Park S, et al., 2012. Improving resolution of miniature spectrometers by exploiting sparse nature of signals. *Opt Expr*, 20(3):2613-2625. https://doi.org/10.1364/oe.20.002613

Oliver J, Lee WB, Lee HN, 2013. Filters with random transmittance for improving resolution in filter-array-based spectrometers. *Opt Expr*, 21(4):3969-3989. https://doi.org/10.1364/oe.21.003969

Pervez NK, Cheng W, Jia Z, et al., 2010. Photonic crystal spectrometer. *Opt Expr*, 18(8):8277-8285. https://doi.org/10.1364/oe.18.008277

Phillips PG, Briotta DA, 1974. Hadamard-transform spectrometry of the atmospheres of Earth and Jupiter. *Appl Opt*, 13(10):2233-2235. https://doi.org/10.1364/AO.13.002233

Rajwade A, Kittle D, Tsai TH, et al., 2013. Coded hyperspectral imaging and blind compressive sensing. *SIAM J Imag Sci*, 6(2):782-812. https://doi.org/10.1137/120875302

Redding B, Liew SF, Sarma R, et al., 2013. Compact spectrometer based on a disordered photonic chip. *Nat Photon*, 7(9):746-751. https://doi.org/10.1038/nphoton.2013.190

Ren WY, Fu C, Arce GR, 2018. The first result of compressed channeled imaging spectropolarimeter. Imaging and Applied Optics, Article JTu4A.21. https://doi.org/10.1364/3D.2018.JTu4A.21

Rueda H, Arguello H, Arce GR, 2015. DMD-based implementation of patterned optical filter arrays for compressive spectral imaging. *J Opt Soc Am A*, 32(1):80-89. https://doi.org/10.1364/JOSAA.32.000080

Shaltout A, Liu JJ, Kildishev A, et al., 2015. Photonic spin Hall effect in gap—plasmon metasurfaces for on-chip chiroptical spectroscopy. *Optica*, 2(10):860-863. https://doi.org/10.1364/optica.2.000860

Soldevila F, Irles E, Durán V, et al., 2013. Single-pixel polarimetric imaging spectrometer by compressive sensing. *Appl Phys B*, 113(4):551-558. https://doi.org/10.1007/s00340-013-5506-2

Sun T, Kelly K, 2009. Compressive sensing hyperspectral imager. Computational Optical Sensing and Imaging, Article CTuA5. https://doi.org/10.1364/COSI.2009.CTuA5

Swift RD, Wattson RB, Decker JA, et al., 1976. Hadamard transform imager and imaging spectrometer. *Appl Opt*, 15(6):1595-1609. https://doi.org/10.1364/AO.15.001595

Takhar D, Laska JN, Wakin MB, et al., 2006. A new compressive imaging camera architecture using optical-domain compression. Computational Imaging IV, Article 606509. https://doi.org/10.1117/12.659602

Vigneau E, Devaux MF, Qannari EM, et al., 1997. Principal component regression, ridge regression and ridge principal component regression in spectroscopy calibration. *J Chemomet*, 11(3):239-249. https://doi.org/10.1002/(SICI)1099-128X(199705)11:3<239::AID-CEM470>3.0.co;2-A

Wagadarikar A, John R, Willett R, et al., 2008. Single disperser design for coded aperture snapshot spectral imaging. *Appl Opt*, 47(10):B44-B51. https://doi.org/10.1364/ao.47.000b44

Wagadarikar AA, Pitsianis NP, Sun XB, et al., 2009. Video rate spectral imaging using a coded aperture snapshot spectral imager. *Opt Expr*, 17(8):6368-6388. https://doi.org/10.1364/oe.17.006368

Wang LZ, Xiong ZW, Gao DH, et al., 2015. Dual-camera design for coded aperture snapshot spectral imaging. *Appl Opt*, 54(4):848-858. https://doi.org/10.1364/ao.54.000848

Wang LZ, Xiong ZW, Shi GM, et al., 2017. Adaptive nonlocal sparse representation for dual-camera compressive hyperspectral imaging. *IEEE Trans Patt Anal Mach Intell*, 39(10):2104-2111. https://doi.org/10.1109/tpami.2016.2621050

Wang Z, Yi S, Chen A, et al., 2019. Single-shot on-chip spectral sensors based on photonic crystal slabs. *Nat Commun*, 10(1):1020. https://doi.org/10.1038/s41467-019-08994-5

Willett RM, Gehm ME, Brady DJ, 2007. Multiscale reconstruction for computational spectral imaging. Computational Imaging V, Article 64980L. https://doi.org/10.1117/12.715711

Wolffenbuttel RF, 2004. State-of-the-art in integrated optical microspectrometers. *IEEE Trans Instrum Meas*, 53(1):197-202. https://doi.org/10.1109/tim.2003.821490

Yetzbacher MK, Miller CW, Boudreau AJ, et al., 2014. Multiple-order staircase etalon spectroscopy. Next-Generation Spectroscopic Technologies VII, Article 910104. https://doi.org/10.1117/12.2049848

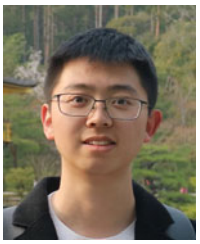

Hongya SONG, first author of this invited paper, received his BS in electronics engineering in 2016 from Wuhan University. He is currently a PhD candidate in optical engineering at Zhejiang University. His research interests include color science, spectral imaging, and computational imaging.

Xiang HAO, corresponding author of this invited paper, is a PI of optical science and technology at Zhejiang University. He received his PhD in optical engineering in 2014 from Zhejiang University. After spending more than four years at Yale University School of Medicine as an associate research scientist, Dr. HAO returned to Zhejiang University in late 2018. He also had short visits at other leading institutes, including Janelia Research Campus of Howard Hughes Medical Institute and University of Oxford. As an optical physicist and biophysicist by training, Dr. HAO has been a long-time contributor to the development of super resolution light microscopy, spectroscopy, photolithography, and applications of these techniques to address biological questions. He is now a corresponding expert of *Front Inform Technol Electron Eng*. He has over 50 peer-reviewed publications and has been granted over 30 patents.